# Butyrate Regulates Liver Mitochondrial Function, Efficiency, and Dynamics in Insulin-Resistant Obese Mice

Maria Pina Mollica,[1] Giuseppina Mattace Raso,[2] Gina Cavaliere,[1] Giovanna Trinchese,[1] Chiara De Filippo,[1] Serena Aceto,[1] Marina Prisco,[1] Claudio Pirozzi,[2] Francesca Di Guida,[2] Adriano Lama,[2] Marianna Crispino,[1] Diana Tronino,[2] Paola Di Vaio,[2] Roberto Berni Canani,[3,4,5] Antonio Calignano,[2] and Rosaria Meli[2]

*Diabetes 2017;66:1405–1418 | DOI: 10.2337/db16-0924*

**Fatty liver, oxidative stress, and mitochondrial dysfunction are key pathophysiological features of insulin resistance and obesity. Butyrate, produced by fermentation in the large intestine by gut microbiota, and its synthetic derivative, the N-(1-carbamoyl-2-phenyl-ethyl) butyramide, FBA, have been demonstrated to be protective against insulin resistance and fatty liver. Here, hepatic mitochondria were identified as the main target of the beneficial effect of both butyrate-based compounds in reverting insulin resistance and fat accumulation in diet-induced obese mice. In particular, butyrate and FBA improved respiratory capacity and fatty acid oxidation, activated the AMPK–acetyl-CoA carboxylase pathway, and promoted inefficient metabolism, as shown by the increase in proton leak. Both treatments consistently increased utilization of substrates, especially fatty acids, leading to the reduction of intracellular lipid accumulation and oxidative stress. Finally, the shift of the mitochondrial dynamic toward fusion by butyrate and FBA resulted in the improvement not only of mitochondrial cell energy metabolism but also of glucose homeostasis. In conclusion, butyrate and its more palatable synthetic derivative, FBA, modulating mitochondrial function, efficiency, and dynamics, can be considered a new therapeutic strategy to counteract obesity and insulin resistance.**

Obesity is a major risk factor for insulin resistance (IR) and type 2 diabetes caused by an imbalance between energy consumption and expenditure that leads to lipid accumulation (1). The excessive energy intake and, particularly, the inadequate fat processing may evoke complex biochemical processes such as inflammation, oxidative stress, and impairment of mitochondrial function (2). The liver plays a central role in the development of obesity-associated metabolic alterations. Indeed, hepatic mitochondrial dysfunction can cause the alteration of fat oxidation, reactive oxygen species (ROS) production, and oxidative stress (3). On the one hand, the increase in ROS production is related to a decrease in mitochondrial uncoupling (4,5). On the other hand, the increase of mitochondrial uncoupling promotes inefficient metabolism, creating an ineffective cycle of glucose and fatty acid oxidation and generating heat instead of ATP (6–8). Therefore, molecules able to modulate mitochondrial function and efficiency are advocated for the prevention/treatment of obesity and IR (9).

Mitochondrial dynamics are closely regulated by fusion and fission homeostasis (10,11), the imbalance of which has been implicated in several metabolic disorders (12–14). Mitochondrial fusion includes the involvement of optic atrophy 1 (Opa1) protein and mitofusin (Mfn) 1 and 2, whereas dynamin-related protein (Drp) 1 and fission protein (Fis) 1 are involved in fission (15). A shift toward fusion optimizes mitochondrial function and is beneficial in the maintenance of long-term bioenergetic capacity. Conversely, a shift toward fission leads to numerous mitochondrial fragments, inducing the autophagy of damaged mitochondria (14,16).

Short-chain fatty acids, the main products of intestinal bacterial fermentation of dietary fibers, have been shown to modulate lipid and glucose metabolism, exerting

[1]Department of Biology, University of Naples Federico II, Naples, Italy
[2]Department of Pharmacy, University of Naples Federico II, Naples, Italy
[3]Department of Translational Medical Science, University of Naples Federico II, Naples, Italy
[4]European Laboratory for Investigation of Food Induced Diseases, University of Naples Federico II, Naples, Italy
[5]CEINGE Advanced Biotechnology, University of Naples Federico II, Naples, Italy

Corresponding author: Rosaria Meli, meli@unina.it.

Received 29 July 2016 and accepted 14 February 2017.

M.P.M. and G.M.R. contributed equally to this work.

antiobesity and antidiabetic effects (17–19). Among these, butyrate has been shown to prevent or treat diet-induced IR in mice (20,21). The butyrate mechanism of action was related to increase of energy expenditure and induction of mitochondrial function in skeletal muscle and brown fat (20).

Butyrate exerts multiple effects by distinct mechanisms; in particular, it acts as a signal molecule, interacting with G protein–coupled receptors free fatty acid (FFA) receptor 2 and 3 (22). Butyrate, as an inhibitor of histone deacetylases activity, may epigenetically regulate gene expression in different diseases, including obesity and metabolic syndrome (23,24).

Indeed, some butyrate-based products are marketed, but their spread is still very limited because the unpleasant taste and rancid smell of butyrate make its oral administration aversive to patients. We previously demonstrated that a synthetic more palatable derivative of butyrate, N-(1-carbamoyl-2-phenyl-ethyl) butyramide (FBA), improves glucose homeostasis and hepatic steatosis in rats fed a high-fat diet (HFD), showing a comparable efficacy with butyrate (21). Here, we have comparatively evaluated the effects of sodium butyrate (butyrate) and FBA on liver glucose metabolism and mitochondrial function, efficiency, and dynamics in a mice model of obesity and IR.

## RESEARCH DESIGN AND METHODS

### Ethics Statement

All procedures involving animals and their care were conducted in conformity with international and national law and policies, including European Union (EU) Directive 2010/63/EU for animal experiments, Animal Research: Reporting of In Vivo Experiments (ARRIVE) guidelines, the Basel Declaration, and the National Centre for the Replacement, Refinement & Reduction of Animals in Research (NC3Rs) concept, and were approved by the Institutional Committee on the Ethics of Animal Experiments (CSV) of the University of Naples Federico II and by the Italian Ministry of Health under protocol No. 2013/0040360.

### Diets and Drugs

The standard diet (STD) had 17% from fat, without sucrose, and the HFD (Teklad #93075), purchased from Harlan, had 45% of energy derived from fat and 7% sucrose. Butyrate was purchased from Sigma-Aldrich (Milan, Italy), and FBA (Italian patent RM2008A000214; April 21, 2008) was provided by Prof. Calignano (Department of Pharmacy, University of Naples Federico II).

### In Vivo Experimental Procedure

Male C57Bl/6 mice (Charles River Laboratories, Calco, Lecco, Italy) were caged in a temperature-controlled room and exposed to a daily 12 h light–12 h dark cycle with free access to STD, unless stated, and drinking water. Young animals (average weight, 26.05 ± 0.62 g) were used. A group ($n$ = 7) was sacrificed at the beginning of the study to establish baseline measurements. At the onset of the study, mice were fed the STD or the 45% HFD. After 12 weeks, the HFD mice were divided into three experimental groups ($n$ = 7): HFD-fed animals and HFD-fed mice treated by gavage with butyrate (100 mg/kg q.d.) or with FBA (212.5 mg/kg q.d., the equimolecular dose of sodium butyrate). STD and HFD mice were orally treated with water as vehicle. All treatments lasted 6 weeks. At the end of the experiment, blood was collected from the inferior cava or portal vein, and serum was obtained for the evaluation of biochemical determinations. The liver was excised and subdivided. Samples not immediately used for mitochondrial preparation were frozen and stored at −80°C for subsequent determinations or were used for transmission electron microscopy and stereology.

### Serum and Hepatic Parameters and Oral Glucose Tolerance Test

Serum alanine aminotransferase (ALT), triglycerides, and cholesterol were measured by the colorimetric enzymatic method using commercial kits (SGM Italia, Rome, Italy; and Randox Laboratories Ltd., Crumlin, U.K.). Lipopolysaccharide (LPS) was measured using the Limulus amebocyte lysate (LAL QCL-1000; Lonza Group Ltd., Basel, Switzerland) technique. Serum interleukin (IL)-1β and IL-10 (Thermo Fisher Scientific, Rockford, IL), tumor necrosis factor-α (TNF-α) and monocyte chemoattractant protein 1 (MCP-1) (Biovendor R&D, Brno, Czech Republic), adiponectin and leptin (B-Bridge International, Mountain View, CA), insulin (cat. no. EZRMI-13K; Millipore, Darmstadt, Germany), and hepatic TNF-α and IL-1β were measured using commercially available ELISA kits. As an index of IR, HOMA-IR was calculated (HOMA-IR = fasting glucose [mmol/L] × fasting insulin [μU/mL]/22.5). In another set of experiments 1 week before mice were killed, an oral glucose tolerance test (OGTT) was measured in mice fasted overnight, as previously described (25).

### Body Composition and Energy Balance

Body weight and food intake were monitored daily to obtain body weight gain and gross energy intake. Energy balance assessments were conducted during the 18 weeks of feeding by the comparative carcass evaluation (26). The gross energy density for the STD or HFD (15.8 or 21.9 kJ/g, respectively) and the energy density of the feces and the carcasses was determined by bomb calorimetric (Parr adiabatic calorimetric; Parr Instrument Co., Moline, IL). Metabolizable energy (ME) intake was determined by subtracting the energy measured in feces and urine from the gross energy intake, which was determined from the daily food consumption and gross energy density. Energy efficiency was calculated as the percentage of body energy retained per ME intake, and energy expenditure was determined as the difference between ME intake and energy gain.

### Mitochondrial Parameters and Basal and Inducible Proton Leak

Mitochondrial isolation, oxygen consumption, and proton leakage measurements were performed as previously reported (27). Oxygen consumption was polarographically measured using a Clark-type electrode in the presence of

substrates and ADP (state 3) or with substrates alone (state 4), and the respiratory control ratio was calculated. Mitochondrial proton leakage was assessed by a titration of the steady-state respiration rate as a function of the mitochondrial membrane potential in liver mitochondria. The specific activity of the carnitine palmitoyltransferase (CPT) system, aconitase, and superoxide dismutase was measured spectrophotometrically, as previously reported (28–30). The rate of mitochondrial $H_2O_2$ release was assayed by measuring the linear increase in fluorescence caused by the oxidation of homovanillic acid in the presence of horseradish peroxidase (31). Mitochondrial protein mass was assessed according to Srere (32).

### Redox Status and Nrf2-Activated Enzyme Activities

Reduced glutathione (GSH) and oxidized glutathione (GSSG) concentrations in the liver were measured with the dithionitrobenzoic acid-GSSG reductase recycling assay (33); the GSH-to-GSSG ratio was used as an oxidative stress marker. To investigate the possible involvement of NF-E2–related factor 2 (Nrf2) in the diet-induced stress, cytoplasmic extracts were prepared from rat liver. The enzymatic activities of glutathione *S*-transferases (GSTs) and quinone oxidoreductase (NQO1) were evaluated spectrophotometrically in liver cytoplasmic extracts (32,34–36).

### Western Blot Analysis

Blots were probed with anti–phosphorylated AMPK-α (cat no. 2535), AMPK-α (cat no. 2532), phosphorylated acetyl-CoA carboxylase (ACC; cat. no. 11818), ACC (cat no. 3676), insulin receptor (cat no. 3025), and phosphorylated AKT (cat no. 4060; Cell Signaling Technology, Danvers, MA), AKT (cat no. sc-5298; Santa Cruz Biotechnology, Dallas, TX), phosphorylated insulin receptor (cat no. 44-800G; Thermo Fisher Scientific, Waltham, MA), and GLUT2 (cat no. 07-1402; Millipore, Temecula, CA). Western blot for β-actin (cat no. A5441) and α-tubulin (cat no. T 9026; Sigma-Aldrich) was performed to ensure equal sample loading.

### Real-time PCR Analysis

Total RNA was extracted from liver using the TRIzol reagent (Ambion). After DNase treatment, RNA was quantified and reverse-transcribed (1 μg) using the Advantage RT-PCR kit (Clontech). For the evaluation of mitochondrial fission and fusion gene transcription, we used murine primers, as follows: *Mfn1*: TCTCCAAGCCCAACATCTTCA (forward), ACT CCGGCTCCGAAGCA (reverse); *Mfn2*: ACAGCCTCAGCCGA CAGCAT (forward), TGCCGAAGGAGCAGACCTT (reverse); *Drp1*: GCGCTGATCCCGCGTCAT (forward), CCGCACCCA CTGTGTTGA (reverse); *Opa1*: TGGGCTGCAGAGGATGGT (forward), CCTGATGTCACGGTGTTGATG (reverse); *Fis1*: GCCCCTGCTACTGGACCAT (forward), CCCTGAAAGCCTCA CACTAAGG (reverse); and *β-Actin*: ACGGCCAGGTCATCAC TATTC (forward), AGGAAGGCTGGAAAAGAGCC (reverse); evaluations were performed as previously described (37). We used mouse primers for *Tnf*, *Il6,* and *Gapdh*, purchased from Qiagen (Hilden, Germany), to evaluate the transcription of inflammatory mediators (38).

### Transmission Electron Microscopy and Stereology

Liver slices were cut into ~1 $mm^3$ fragments, fixed by immersion in 2.5% glutaraldehyde, 2.5% paraformaldehyde in phosphate buffer (0.1 mol/L, pH 7.4) for 2 h at room temperature, postfixed with 1% osmium tetroxide in 0.1 mol/L phosphate buffer for 2 h at 4°C, dehydrated through graded alcohols (50, 70, 90, and 100%) and propylene oxide, and then embedded in Epon 812 resin (48 h at 60°C). Ultrathin (70 nm thick) sections were cut on a Sorvall Porter-Blum ultramicrotome and examined on a Philips 208S transmission electron microscope. Micrographs were acquired with a Mega View II Soft Imaging System. For each experimental group, 30 random images were taken at original magnification ×25,000 for mitochondria investigation and at original magnification ×4,000 for lipid investigation. We used the point-sampling technique of classic stereology to measure mitochondrial density and lipid volume density (39,40). Briefly, a grid with equally and symmetrically spaced intersection points was overlaid on each micrograph using ImageJ 1.50 software (National Institutes of Health). Mitochondrial and lipid volume density was calculated as the ratio of points overlapping the cellular compartment of interest and the total number of grid points overlapping the cytoplasm area. The values are expressed as the percentage ± SEM.

Mitochondrial morphological characteristics were quantified: mitochondrial area, aspect ratio (the ratio between the major and minor axis of the ellipse equivalent to the mitochondrion), degree of branching or form factor (defined as $[Pm^2]/[4\pi Am]$, where Pm is the length of mitochondrial outline and Am is the area of mitochondrion), mitochondrial density ($N/\mu m^2$), and coverage (percentage of cytosol). For mitochondrial area, 400 mitochondria/sample were counted; for other parameters, 10 photos/sample were analyzed.

### Cell Culture

Human Hep G2 cells (American Type Culture Collection, Manassas, VA) were cultured in RPMI 1640 medium supplemented with 10% FBS and 1% antibiotics (100 units/mL penicillin and streptomycin) at 37°C with 5% $CO_2$.

Hep G2 cells, starved in serum-free medium for 16 h, were incubated with insulin (100 nmol/L) or its vehicle for 24 h to obtain IR and control cells, respectively (41). To evaluate butyrate effect, control and IR cells were simultaneously treated with sodium butyrate (1 mmol/L). After 24 h, cells were washed and then challenged with 100 nmol/L insulin for 10 min to determine the insulin signaling pathway or 6 h for GLUT2 determination.

### Statistical Analysis

Data are presented as the means ± SEM unless otherwise indicated. Differences among groups were compared by ANOVA, followed by the Newman-Keuls test for multiple comparisons. Differences were considered statistically significant at $P < 0.05$. Analyses were performed using GraphPad Prism (GraphPad Software, La Jolla, CA).

## RESULTS

### Butyrate and FBA Reduced Lipid Accumulation, Lowering Body Energy Efficiency and Increasing Energy Expenditure

The mean body weight of all mice groups, measured during the entire experimental period, is shown in Fig. 1*A*. HFD feeding clearly led to a significant increase in body weight throughout the experiment. Butyrate or FBA treatment, starting at week 12, significantly reduced body weight. These data were confirmed by the area under curve (AUC) of body weight, calculated from 12 to 18 weeks (Fig. 1*B*). Evaluation of body water revealed a decrease in HFD-fed mice that was partially restored only in the FBA group (Fig. 1*C*). Moreover, we found that HFD-fed animals exhibited an increase in body lipids percentage and energy, which was partially reverted by butyrate and to a larger

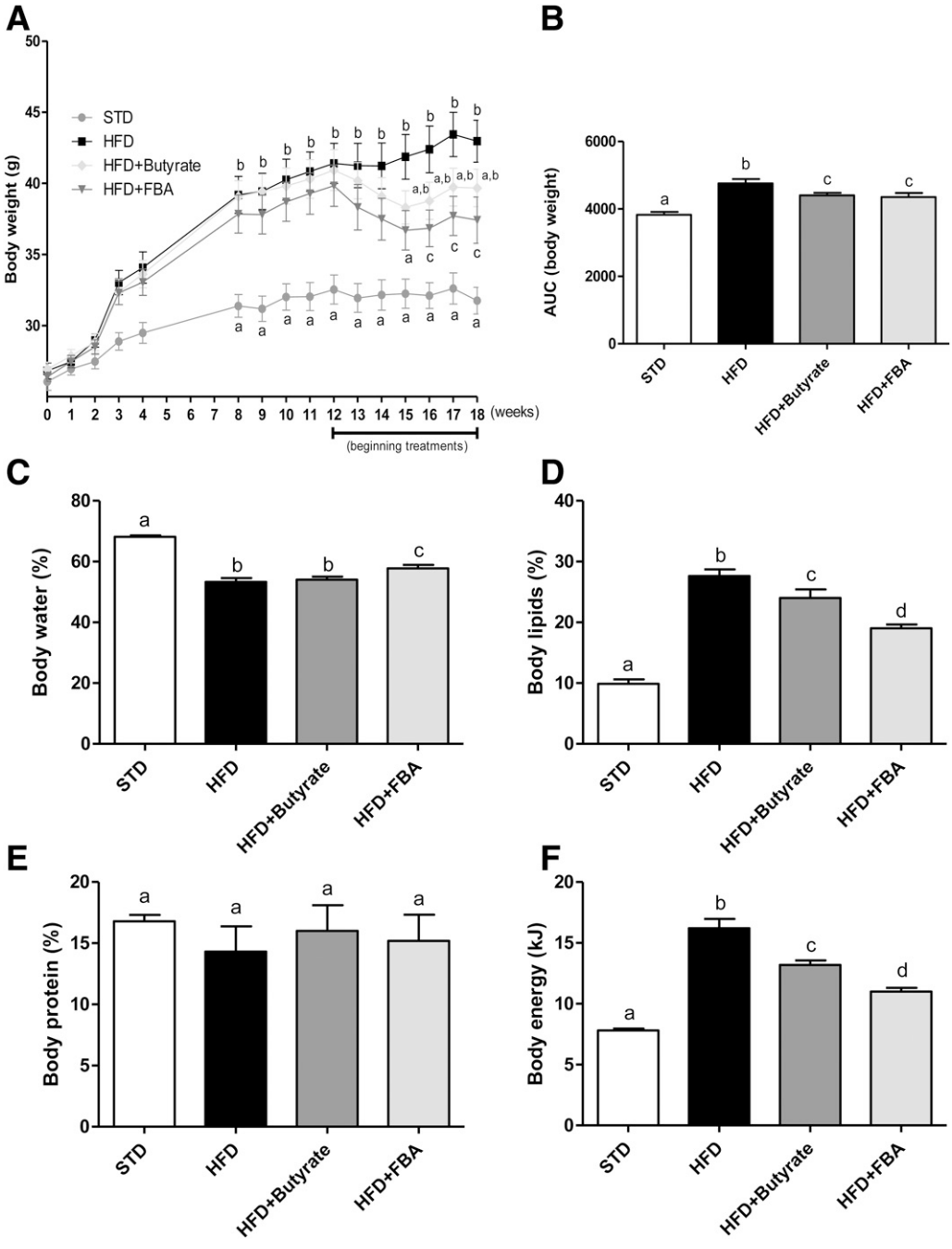


**Figure 1**—Butyrate and FBA treatment induced body weight modification and composition in diet-induced obese mice. Body weight measured throughout the experimental period (*A*) and AUC of body weight during the study period (12 to 18 weeks) (*B*). Body water (*C*), lipid (*D*), and protein (*E*) percentages and energy in kJ (*F*) are reported. Data are presented as means ± SEM from $n = 7$ animals/group. Labeled means without a common letter differ, $P < 0.05$.

extent by FBA (Fig. 1*D* and *F*). No variation was observed in body protein content (Fig. 1*E*).

All groups fed the HFD showed a similar energy intake (data not shown); however, when this parameter is reported as kJ/100 g mice/week (Fig. 2*A*), it resulted in an increase in butyrate- and FBA-treated mice. Fecal energy decreased in all HFD groups (Fig. 2*B*), and no difference was reported in urine energy among all groups (data not shown). All HFD-fed groups showed a similar ME intake higher than the STD-fed mice (Fig. 2*C*). In the HFD group, we found an increase in body weight gain (Fig. 2*D*), lipid gain (Fig. 2*E*), and lipid gain/ME intake (Fig. 2*F*) compared with the STD group, and all of these parameters were reduced by butyrate and more deeply by FBA. Butyrate and FBA showed a significant reduction in energy efficiency compared with HFD mice (Fig. 2*H*) and a significant increase in energy expenditure (Fig. 2*G*). Probably, the strongest effect of FBA on body lipids was related to a lower energy efficiency (Fig. 2*H*). No modification was shown in protein gain or protein gain/ME intake (Fig. 2*I* and *J*). Taken together, these data indicate that butyrate- and FBA-treated mice had an improved capability to utilize fat as a metabolic fuel.

### Butyrate and Its Derivative, FBA, Modulated Serum and Hepatic Inflammatory Markers and Metabolic Parameters

Serum triglycerides, cholesterol, and ALT were significantly increased by the HFD compared with the STD and were reduced by butyrate and FBA (Fig. 3*A* and *B*). Similarly, the hormonal profile altered by the HFD was improved by both butyrate-based treatments, as shown by leptin and adiponectin serum levels (Fig. 3*C* and *D*). The increased proinflammatory serum markers, such as TNF-α, MCP-1, and IL-1β were significantly reduced in butyrate-treated animals and even more by FBA (Fig. 3*E–G*). Consistently, the highest endotoxemia found in the HFD mice was reduced by both treatments (Fig. 3*H*). The anti-inflammatory effect of butyrate and FBA was also shown at the hepatic level on the cytokine transcription and protein level (Fig. 3*I–M*).

### Butyrate and FBA Improve Insulin Sensitivity and Glucose Homeostasis

Glucose tolerance and IR were studied to analyze the effects of butyrate and FBA on glucose homeostasis in HFD-fed mice. As expected, the HFD induced a marked and significant increase of glycemia in the OGTT ($P < 0.001$) and AUC values, which was significantly reduced by butyrate and FBA (Fig. 4*A*). Butyrate and FBA groups exhibited improved tolerance to glucose at all time points. No difference in fat mass and body weight was evidenced in STD mice treated or not with butyrate-based compounds (data not shown). Conversely, glucose tolerance was improved in butyrate-treated STD mice, evaluated as AUC values expressed as glucose/min (18,525 ± 642 butyrate and 19,871 ± 575 FBA vs. 21,150 ± 573 STD). Compared with STD mice, HFD mice showed a marked increase in fasting glucose and insulin level prevented by both butyrate and FBA (Fig. 4*B* and *C*, respectively), improving HOMA-IR (Fig. 4*D*). Furthermore, the evaluation of the AMPK-α/ACC pathway activation in liver revealed a marked upregulation in the phosphorylated AMPK protein and its downstream substrate ACC both in butyrate- and FBA-treated mice (Fig. 4*E* and *F*). Both treatments similarly induced an increase in AKT phosphorylation compared with HFD mice as well as an upregulation of GLUT2 expression markedly reduced by the HFD (Fig. 4*G* and *H*).

To address the direct effect of butyrate on hepatic insulin sensitivity, we evaluated the modulation of insulin signaling and GLUT2 expression altered by the induction of IR in human Hep G2 cells. We have demonstrated that butyrate increases the phosphorylation of insulin receptor and Akt, as well as GLUT2 expression, after insulin stimulation (Fig. 4*I–K*).

### Mitochondrial Efficiency and Oxidative Stress Modulation by Butyrate-Based Treatments

Mitochondrial state 3 respiration, evaluated using succinate as the substrate, was decreased in HFD-fed animals compared with the other groups (Fig. 5*A*). To study fatty acid oxidation, state 3 respiration was evaluated using palmitoyl-carnitine as the substrate; butyrate and FBA increased oxygen consumption compared with STD and HFD groups (Fig. 5*B*). No variation was observed in mitochondrial state 4 respiration among all groups using succinate or palmitoyl-carnitine substrate (Fig. 5*A* and *B*, respectively) and in CPT activity (Fig. 5*C*). High quality of mitochondrial preparations was indicated by high respiratory control ratio values in all groups (data not shown).

As depicted in Fig. 5*D*, the specific activity of citrate synthase, significantly reduced compared with controls in HFD liver homogenates, was increased by butyrate and restored by FBA. Conversely, citrate synthase activity in isolated liver mitochondria was similar in all groups. Interestingly, mitochondrial protein contents, calculated as the ratio between citrate synthase activity in the homogenate and isolated mitochondria, was significantly lower in the HFD group compared with all groups, and butyrate and, even more, FBA significantly increased this parameter (Fig. 5*D*).

In mitochondrial basal conditions or after FFA stimulation, HFD showed the lowest proton leak, which was increased by butyrate and FBA compared with STD and HFD (Fig. 5*E* and *F*). In particular, mice treated with both formulations exhibited the highest oxygen consumption to maintain the same membrane potential among the groups (Fig. 5*E*). Regarding FFA-induced proton leak, FBA mice showed a better efficacy than butyrate mice (Fig. 5*F*).

Next, $H_2O_2$ yield and ROS-induced damage were measured in isolated mitochondria. The $H_2O_2$ yield was increased in the HFD group compared with the STD group and was significantly decreased in butyrate- and FBA-treated mice (Fig. 5*G*). Similarly, HFD mice showed a lower aconitase activity, which was increased by butyrate or FBA (FBA > butyrate) (Fig. 5*H*).

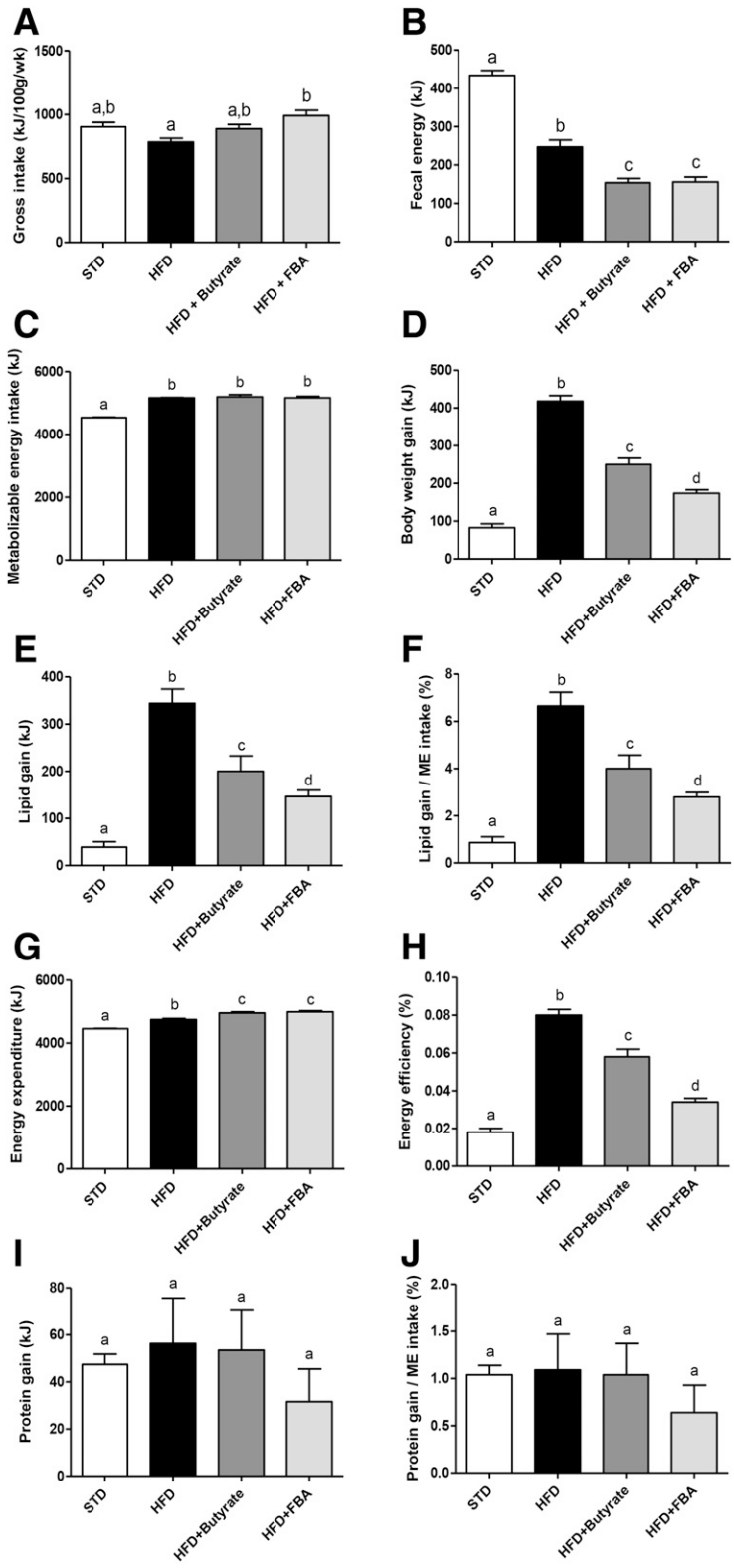


**Figure 2—**Butyrate and FBA treatments reduced body weight gain, lipid gain, and energy efficiency in diet-induced obese mice. Gross intake (*A*), fecal energy (*B*), ME intake (*C*), body weight gain (*D*), lipid gain (*E*), lipid gain/ME intake (*F*), energy expenditure (*G*) and efficiency (*H*), protein gain (*I*), and protein gain/ME intake (*J*) were measured in STD, HFD, and HFD animals treated with butyrate or FBA. Data are presented as means ± SEM from $n = 7$ animals/group. Labeled means without a common letter differ, $P < 0.05$.

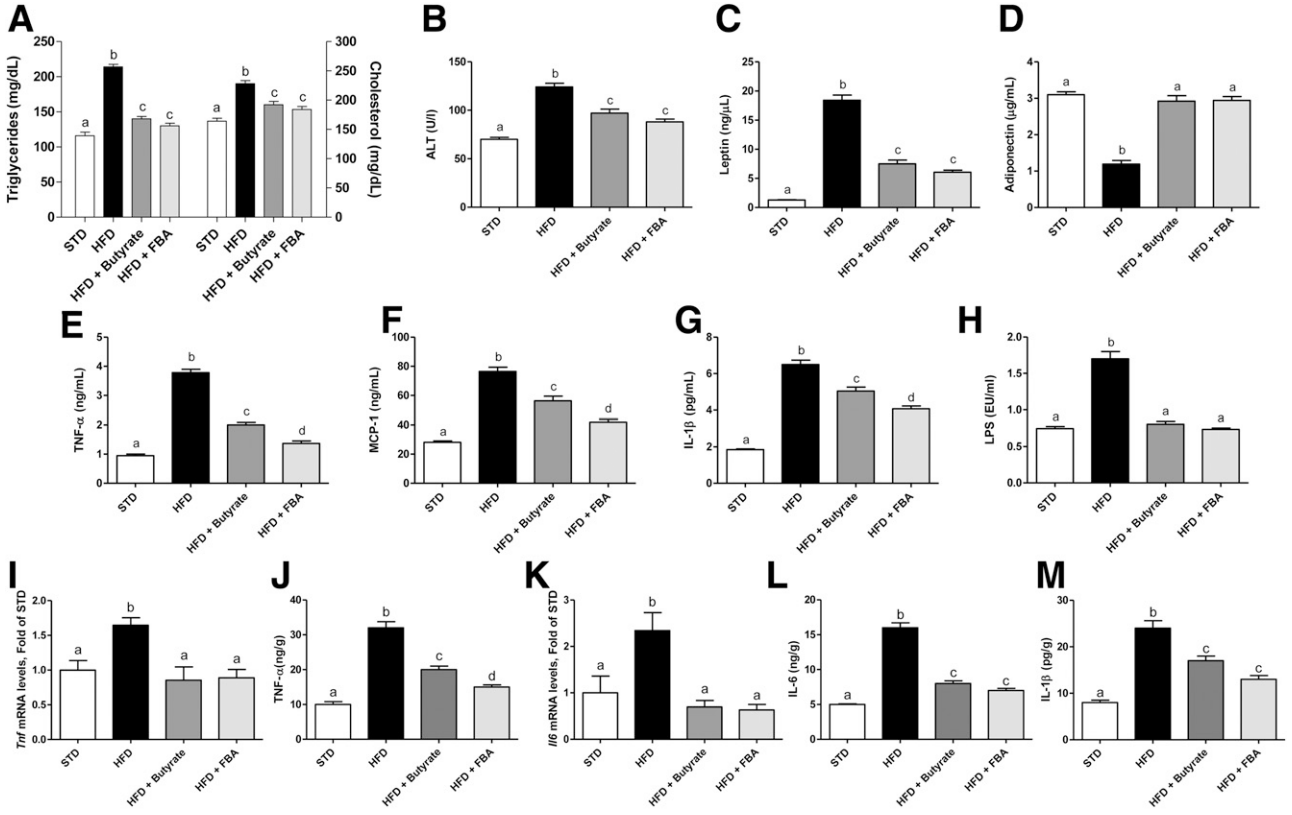


**Figure 3**—Butyrate and FBA restore serum metabolic parameters and reduce proinflammatory markers in serum and the liver. Metabolic parameters, such as triglycerides and cholesterol (*A*), ALT (*B*), leptin (C), and adiponectin (*D*), and proinflammatory cytokines, such as TNF-α (*E*), MCP-1 (*F*), IL-1β (*G*), and LPS (*H*), are measured in serum. *Tnf* (I) and *Il6* (*K*) gene expression in the liver was evaluated. Hepatic TNF-α (*J*), IL-6 (*L*), and IL-1β (*M*) were also measured. Data are presented as means ± SEM from $n = 7$ animals/group. Labeled means without a common letter differ, $P < 0.05$.

### Antioxidant/Detoxifying Effect by Butyrate-Based Treatments

Antioxidant state and cytoprotective enzyme activity were improved by butyrate or FBA administration (Fig. 6). Nrf2 is considered the main mediator of cellular adaptation to redox stress, and its translocation into the nucleus, upon the dissociation from the Kelch-like ECH-associated protein 1 (Keap1), triggers the transcription of several enzymes involved in detoxification and chemopreventive mechanisms (GSTs, NAD[P]H, NQO1). In particular, NQO1 and GST activity, as well as GSH level, were significantly lower in HFD mice compared with STD mice. Butyrate treatment increased all parameters, and this effect was more marked in FBA-treated mice (Fig. *6A–C*). GSSGs were higher in all HFD-fed groups compared with STD-fed groups (Fig. 6*D*). The beneficial effects on liver redox status induced by butyrate, and more markedly by FBA treatment, were clearly indicated by the significant increase of the GSH-to-GSSG ratio (Fig. 6*E*).

### Electron Microscopy and Modulation of Lipid Content by Butyrate-Based Treatments

Lipid droplets were evident in the liver sections of all HFD groups; however, their size and content in the HFD groups were higher than in the treated groups (Fig. 7*A*). Consistently, stereology investigations revealed that lipid density was significantly decreased compared with HFD mice in the butyrate groups and even more in FBA groups (Fig. 7*C*).

In the liver of the HFD mice, mitochondrial dumbbell-shaped and fission pictures are evident, while an ongoing fusion event is shown in butyrate-treated mice; giant and elongated mitochondria, resulting from fusion, are recognizable in the FBA group (Fig. 7*B*). Mitochondrial area and volume density were significantly lower in the HFD group compared with the other groups (Fig. 7*D* and *E*). The mitochondrial aspect ratio (the length of mitochondria), density, and form factor (an index of the degree of mitochondrial branching) were significantly increased in HFD mice compared with all other groups (Fig. 7*F–H*). Finally, mitochondrial coverage (percentage of cytosol) results were significantly decreased in HFD and butyrate livers and recovered in FBA (Fig. 7*I*). The increased mitochondrial volume density showed by butyrate and FBA was probably associated to the decreased lipid compartment.

### Effect of Butyrate and FBA on Mitochondrial Dynamics

Mitochondrial dynamics, fission and fusion, is a metabolic process dedicated to cell energy demand modulation. As

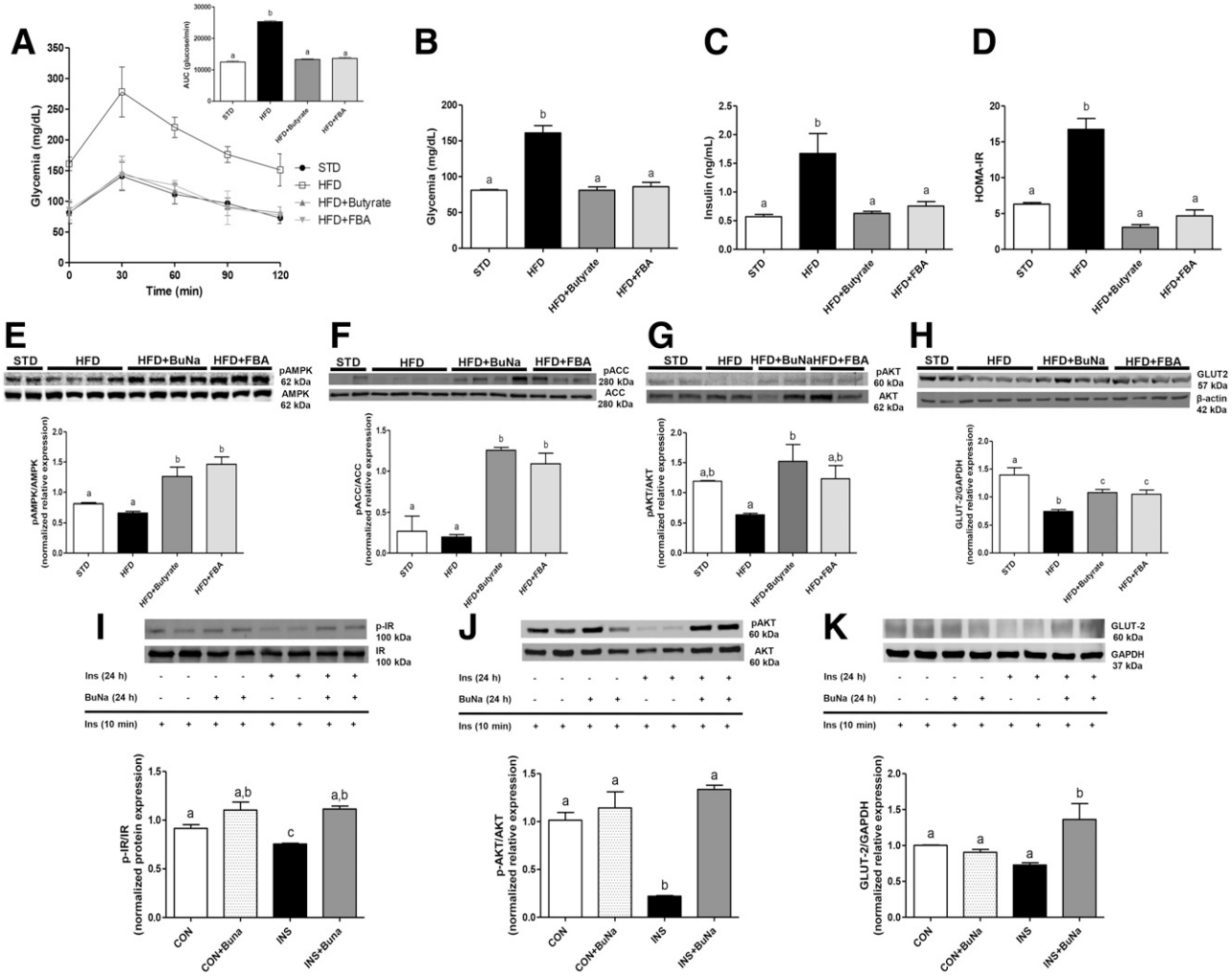


**Figure 4—**Butyrate and FBA improve body glucose homeostasis and IR. *A*: OGTT in STD- and all HFD-fed groups was performed. Fasting glucose (*B*), insulin levels (*C*), and HOMA-IR (*D*) are reported. Data are presented as means ± SEM from $n = 7$ animals/group. Liver phosphorylated (p)AMPK-to-AMPK (*E*), pACC-to-ACC (*F*), and pAKT-to-AKT (*G*) ratios and GLUT2 expression (*H*) were also evaluated by Western blot and densitometric analysis ($n = 6$ for each group). The pIR-to-IR (*I*) and pAKT-to-AKT (*J*) ratios and GLUT2 expression (*K*) were also evaluated in Hep G2. Cells were stimulated or not with insulin (100 nmol/L) for 24 h, with or without butyrate (1 mmol/L). CON, control cells; CON+BuNa, control cells treated with sodium butyrate; INS, insulin-resistant cells; INS+BuNa, insulin-resistant cells treated with butyrate. After washout, all cells were stimulated with insulin for 10 min to evaluate phosphorylated proteins or for 6 h for GLUT2 expression. Data are from triplicate experiments. Labeled means without a common letter differ, $P < 0.05$.

shown in Fig. 8*A–C*, we found a significant reduction in fusion protein mRNAs, namely, *Mfn1*, *Mfn2*, and *Opa1*, in the liver from HFD mice compared with STD mice, and a significant increase in their transcription was revealed in butyrate- or FBA-treated animals. The transcription of fission proteins *Drp1* and *Fis1* was consistently reduced in butyrate- or FBA-treated mice, as shown in Fig. 8*D* and *E*, respectively.

## DISCUSSION

The main finding of this study is that the administration of butyrate or FBA in mice fed the HFD reduces hepatic fat accumulation and decreases metabolic/mitochondrial efficiency, counteracting obesity, IR, and inflammation. A relevant role for hepatic mitochondria has been evidenced, as the main target of diet-induced alterations in function, efficiency, and dynamics, associated to an increase of oxidative stress and inhibition of the Nrf2 pathway.

The HFD increases metabolic efficiency, weight gain, and body lipid levels, leading to metabolic alterations, such as dyslipidemia and IR, associated with low-grade inflammation. Despite comparable ME intake in all mice fed the HFD, we found a reduction in metabolic efficiency, body weight, and body lipid levels after butyrate and FBA treatments. The butyrate and FBA effects on body weight and lipids can be at least partly explained by an increase in energy expenditure and reduced energy efficiency. Butyrate and FBA improve the ability to utilize fat as a metabolic fuel, suggesting that the large part of the higher energy intake was dissipated through increased metabolic activity.

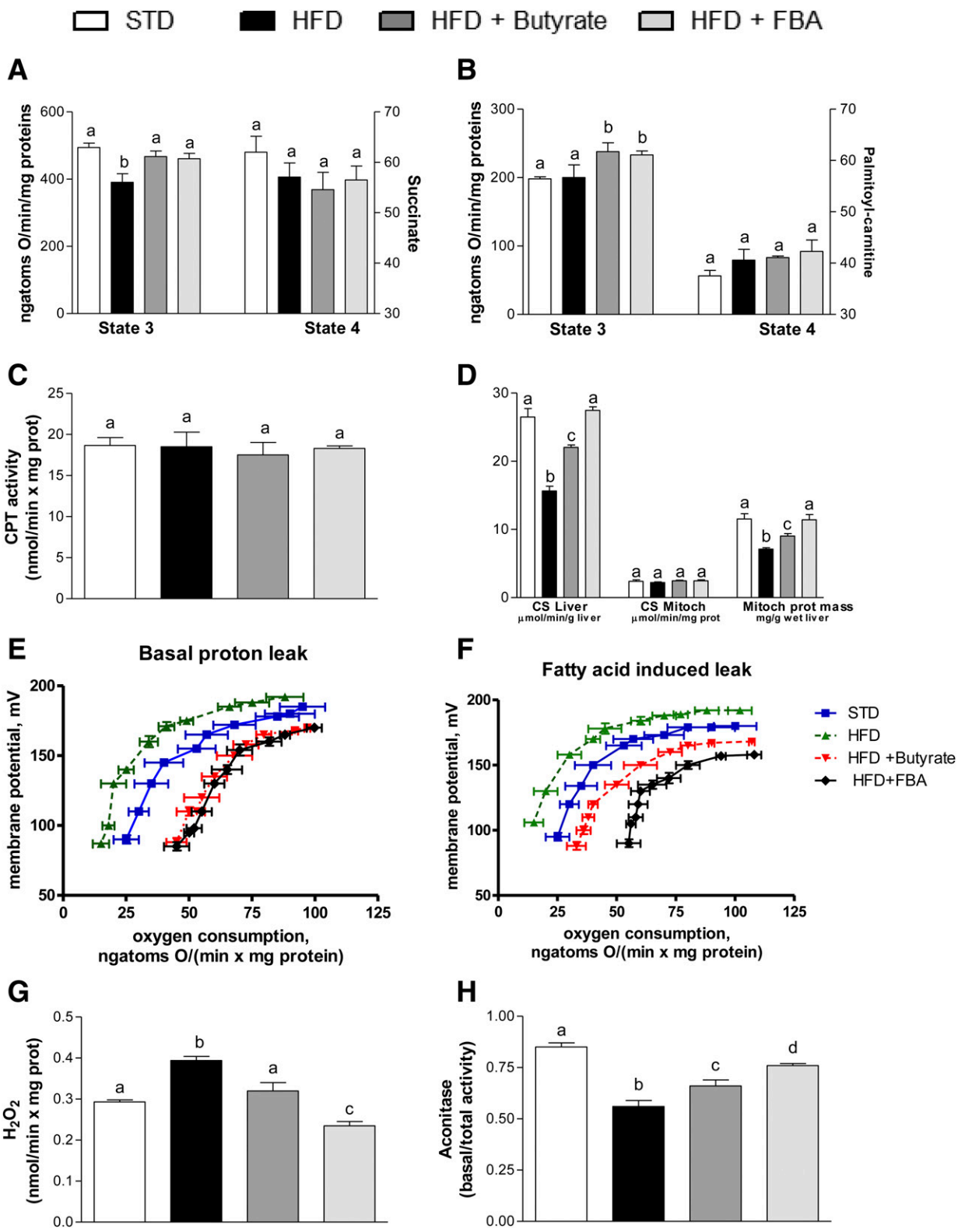


**Figure 5**—Effect of butyrate and FBA on liver mitochondrial function and energy efficiency. Mitochondrial respiration in the presence of succinate (*A*) or palmitoyl-carnitine (*B*) as substrates was determined. CPT activity (*C*) and citrate synthase (CS) activity was determined in liver homogenates and in mitochondria isolated and mitochondrial protein mass (*D*). Basal (*E*) and palmitate-induced (*F*) proton leakage in mitochondria, $H_2O_2$ yield (*G*), and aconitase activity (*H*) are also shown. Data are presented as means ± SEM from $n = 7$ animals/group. Labeled means without a common letter differ, $P < 0.05$.

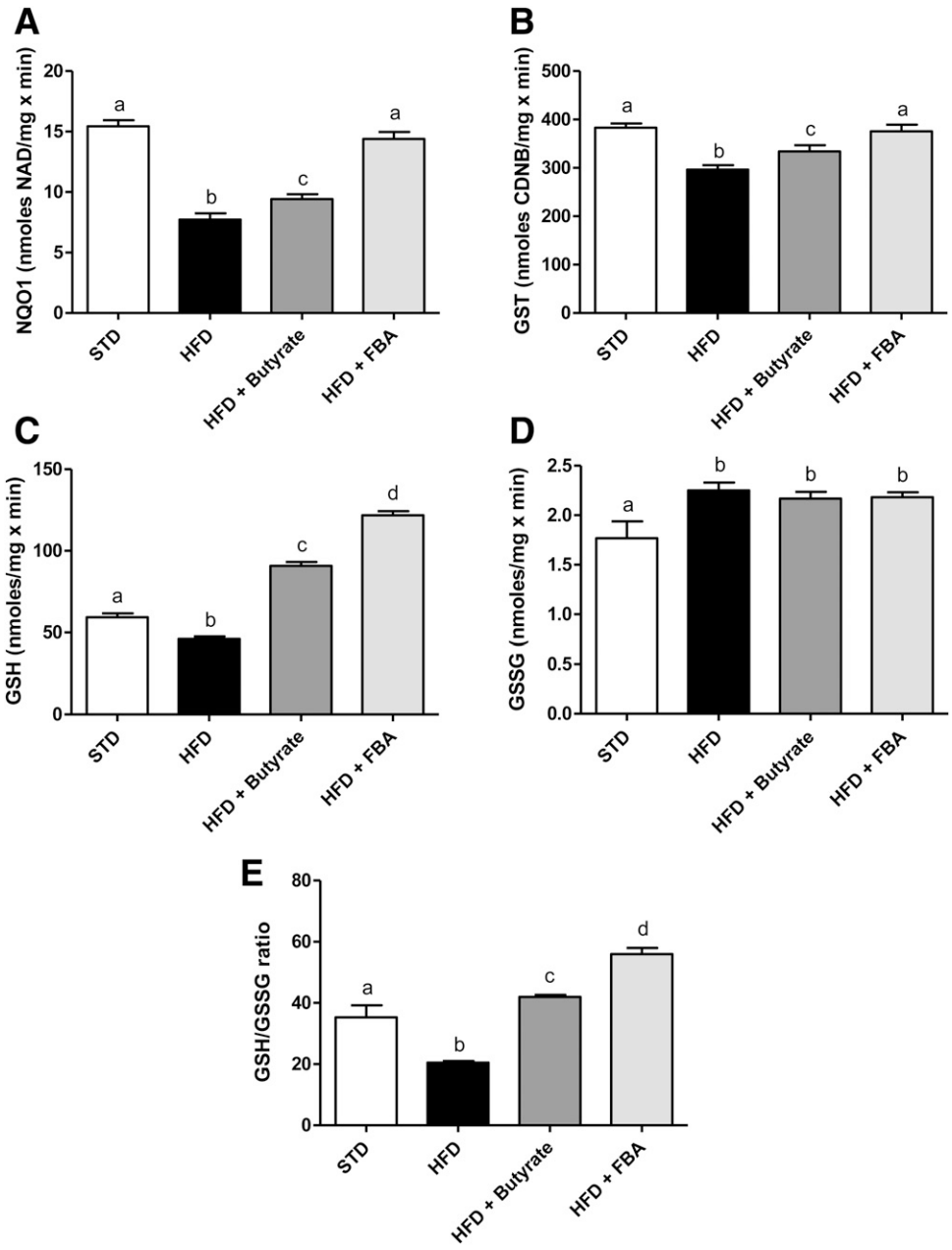


**Figure 6**—Butyrate and FBA improve antioxidant/detoxifying defense. NQO1 (*A*) and GST (*B*) activity, GSH (*C*) and GSSG (*D*) content, and the GSH-to-GSSG ratio (*E*) are shown. The data are presented as means ± SEM from $n = 7$ animals/group. Labeled means without a common letter differ, $P < 0.05$.

Butyrate and FBA attenuated HFD-induced alteration of lipid and hormonal profiles, restoring glucose homeostasis and liver GLUT2 expression and reducing inflammation. Both treatments also counteracted adiponectin and leptin alterations, adipokines that are inversely involved in glucose and lipid metabolism, through AMPK activation (42,43). Our results showed decreased serum leptin levels in butyrate- and FBA-treated mice, consistent with fat mass reduction, and serum adiponectin levels restored to those of STD mice, associated with AMPK/ACC pathway activation and fatty acid metabolism in the liver. Notably, the activation of AMPK exhibits multiple effects, including a reduction in inflammation, oxidative stress, and IR and an increase in lipid metabolism (43,44). The anti-inflammatory effect of butyrate and FBA at the hepatic level could also be ascribed to a reduction in gut leakage, as suggested by the reduction of LPS levels in portal blood, in accordance with our recent findings showing that both butyrate-based compounds restored gut integrity in mice with dextran sulfate sodium–induced colitis (45), contributing to immune tolerance (46). Our previous data demonstrated that butyrate and FBA, in rats fed the HFD, reduced hepatic proinflammatory parameters via suppression of Toll-like receptors and nuclear factor-κB activation in the liver (21).

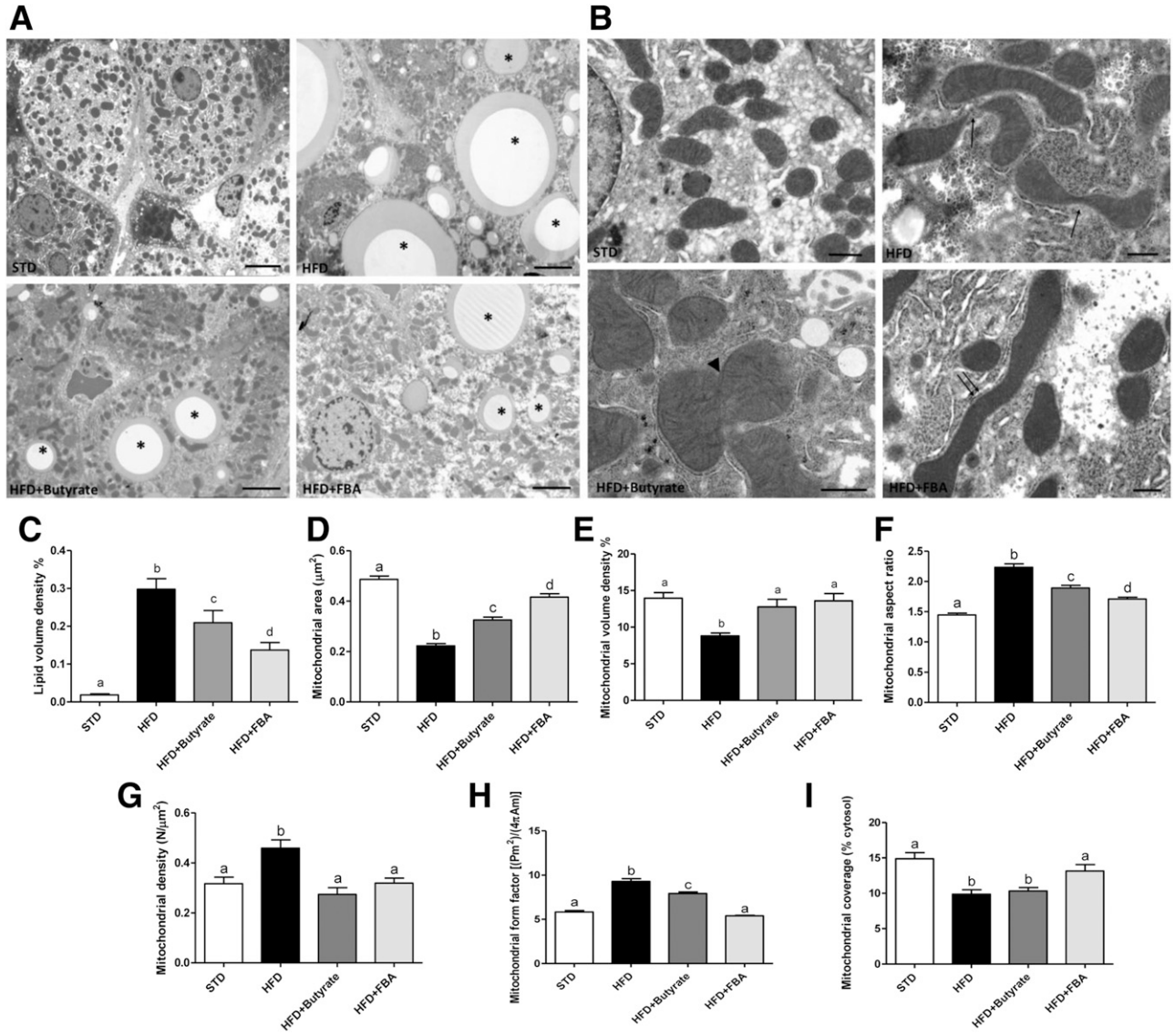


**Figure 7**—Electron microscopy and stereology of liver sections. *A*: Representative images of the liver from all HFD groups are shown; lipid droplets are visible (*), differently from STD. In HFD-fed mice, the lipids are more abundant and larger than in butyrate- and FBA-treated mice. Bars = 5 μm. *B*: Shape and size of liver mitochondria are reported. Mitochondrial dumbbell-shaped and fission pictures (arrows) are shown in HFD-treated mice, and fusion events (arrowhead) are recognizable in the cytoplasm of butyrate-treated mice, resulting in giant and elongated mitochondria (double arrows) in the FBA group. Bars: STD = 1 μm; other groups = 0.5 μm. Lipid volume density (*C*), mitochondrial area (*D*), volume density (*E*), aspect ratio (*F*), density (*G*), form factor (*H*), and coverage (*I*) are also shown. Labeled means without a common letter differ, $P < 0.05$.

Furthermore, we address the direct effect of butyrate on hepatocyte insulin sensitivity, demonstrating the reversal of IR in insulin-stimulated Hep G2 cells through the restoration of hormone signaling and GLUT2 expression.

Our data confirm the association between HFD-induced ectopic fat storage in the liver and alterations in the mitochondrial compartment (47). Accordingly, liver mitochondria from the HFD mice exhibited reduced mitochondrial protein mass, area, volume density, and respiratory capacity and increased oxidative stress, even when the ability to utilize palmitoyl-carnitine as a fat metabolic fuel was unchanged. However, unchanged lipid oxidation is likely not sufficient to counteract the increased FFA overload, leading to the increase of hepatic ectopic lipid storage, as shown by stereology analysis. Moreover, a further mechanism converging to fat accumulation is related to the increase in mitochondrial efficiency, as shown by the decrease in proton leak in the HFD mice. Therefore, the observed higher mitochondrial efficiency is suggestive of a reduced amount of substrate to be burned to obtain ATP. Moreover, increased mitochondrial oxidative stress was found in HFD mice, as shown by $H_2O_2$ yield, aconitase activity, and the GSH-to-GSSG ratio. All of these effects can be attributable to the concomitant increase in NADH and flavin adenine dinucleotide generation, and thus, electron delivery to the respiratory chain, as a

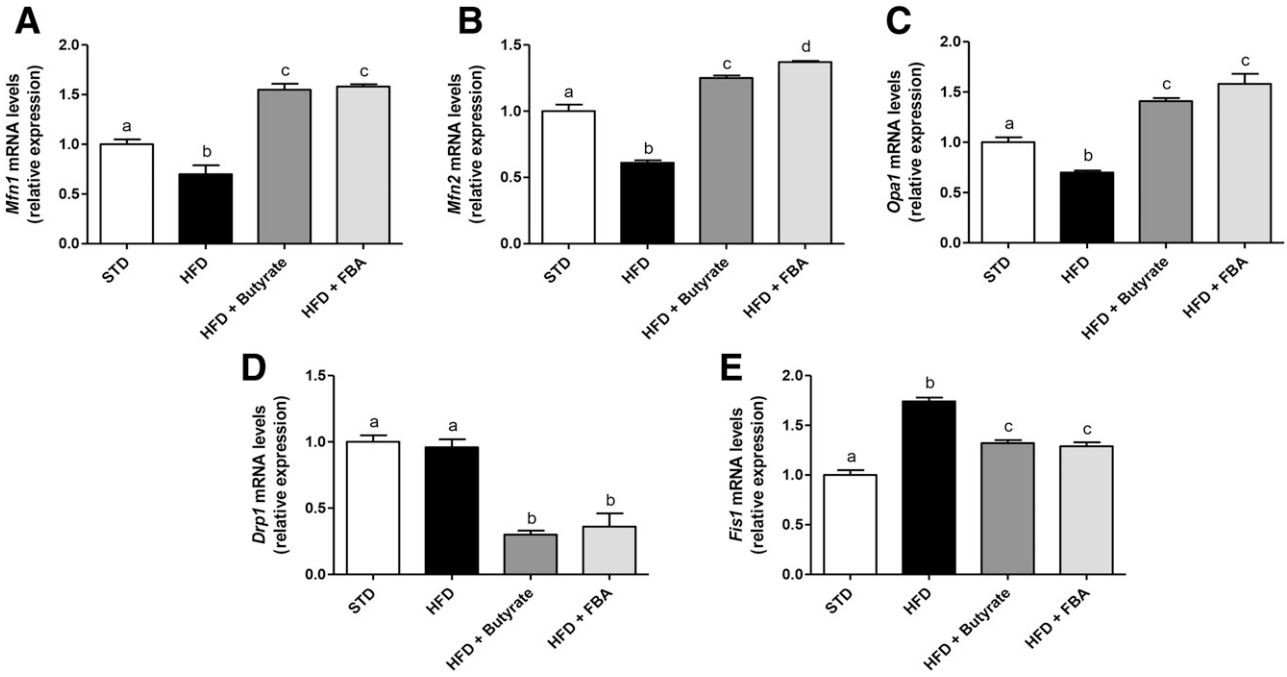


**Figure 8**—Effect of butyrate and FBA on mitochondrial fusion and fission gene transcription. The expression level of the genes *Mfn1* (*A*), *Mfn2* (*B*), and *Opa1* (*C*) is reduced in HFD mice compared with STD but increases in butyrate- and FBA-treated animals. The expression level of the genes *Drp1* (*D*) and *Fis1* (*E*) is also shown. These transcripts were reduced in butyrate- and FBA-treated mice compared with HFD mRNA levels. Data are presented as means ± SEM from $n = 5$ animals/group. Labeled means without a common letter differ, $P < 0.05$.

result of the diet-induced increase of FFA uptake associated to respiratory chain impairment. The decrease in succinate state 3 oxygen consumption partially blocks electron flow within the respiratory chain. Moreover, the decreased proton leak can contribute to excessive ROS formation in HFD mice. In fact, one of the postulated roles of uncoupling is known to be the maintenance of mitochondrial membrane potential below the critical threshold for ROS production (48,49).

The protective effect of butyrate and FBA on liver IR may be the result of multiple mechanisms: the increase in mitochondrial protein mass, area, and volume density, the improvement of respiratory capacity and fatty acid oxidation, and the decrease in mitochondrial efficiency, in accordance with the decrease in body metabolic efficiency and the increase in energy expenditure. Moreover, the Nrf2-mediated adaptive response triggered by mild oxidative stress has been reported as a key protective mechanism against several toxic insults (50). We provide indirect evidence that butyrate and FBA improve liver redox status and cytoprotective defenses through a typical adaptive response.

Morphological parameters analysis indicates that the HFD presents mitochondrial alterations that were often restored by butyrate and FBA treatment. The recovery of glucose homeostasis by butyrate and FBA may be also related to the modification of mitochondrial dynamics. In particular, the fusion process is consistently related to an improvement of IR (14,16). Notably, here butyrate and FBA modulate the proteins involved in mitochondrial dynamics, indicating a clear shift toward the fusion process (MFN1, MFN2, and OPA1), associated with a decrease in DRP1 and FIS1, which are generally transcribed during fission. All these proteins were similarly modulated by butyrate and FBA and even more by FBA for MFN2. This latter protein controls not only mitochondrial cell energy metabolism but also insulin signaling by limiting ROS production (14) and is stringently modulated by several factors. In fact, proinflammatory cytokines and lipid availability reduced its expression, whereas exercise and increased energy expenditure promoted its upregulation (14,51). These results on mitochondrial dynamics were also confirmed by electron microscopy, where clear fission mitochondria were observed in HFD livers, whereas giant and elongated mitochondria, peculiar to fusion, were revealed in butyrate groups. Actually, mitochondrial fusion and uncoupling are two protective mechanisms that reduce oxidative stress, improve mitochondria health and function, and are both modulated by butyrate and FBA. In mitochondrial dynamics, a shift toward fusion maintains a long-term bioenergetic capacity because it favors the generation of interconnected mitochondria, responsible for uncoupling effect that contributes to the rapid energy dissipation. Conversely, a shift toward fission results in numerous mitochondrial fragments, where the mix of the matrix and the inner membrane allows the respiratory machinery components to cooperate most efficiently. Bach et al. (52) consistently demonstrated a decreased mitochondrial proton leak and increased bioenergetics efficiency in Mfn2-depleted cells. Moreover, Mfn2

loss of function enhanced bioenergetic efficiency and contributed to obesity development by reducing energy expenditure and increasing fat energy store (16). Indeed, the complete mechanisms of mitochondrial dynamics are still far from being understood. Very recently, the direct relation between the increase in fusion and IR/obesity has been evidenced, possibly identifying the mitochondrial fission as an adaptive mechanism to cope with lipid overflow (53).

In conclusion, butyrate and FBA promote inefficient metabolism, generating heat instead of ATP, increasing lipid oxidation, activating the AMPK/ACC pathway, reducing ROS generation, and modulating mitochondrial efficiency and dynamics; therefore, they reduce fat mass, inflammation, and IR associated with fat overnutrition.

**Acknowledgments.** The authors thank Giovanni Esposito and Angelo Russo, of the Department of Pharmacy, and Dr. Roberta Scognamiglio, of the Department of Biology, University of Naples Federico II, for animal care and technical assistance.

**Duality of Interest.** No potential conflicts of interest relevant to this article were reported.

**Author Contributions.** M.P.M., G.M.R., and R.M. conceived and designed the experiments, analyzed data, and wrote the manuscript. G.C., G.T., C.D.F., S.A., C.P., F.D.G., A.L., and P.D.V. performed experiments, collected data, and performed data analyses. M.P. performed microscopy analysis. M.C., R.B.C., and A.C. contributed to the discussion and review and to editing of the manuscript. D.T. synthesized FBA. R.M. is the guarantor of this work and, as such, had full access to all the data in the study and takes responsibility for the integrity of the data and the accuracy of the data analysis.

**Prior Presentation.** Parts of this study were presented in poster form at the 37th National Meeting of the Italian Society of Pharmacology, Naples, Italy, 27–30 October 2015.

## References

1. Stein CJ, Colditz GA. The epidemic of obesity. J Clin Endocrinol Metab 2004; 89:2522–2525
2. Hernandez-Aguilera A, Rull A, Rodriguez-Gallego E, et al. Mitochondrial dysfunction: a basic mechanism in inflammation-related non-communicable diseases and therapeutic opportunities. Mediators Inflamm 2013;2013:135698
3. Nakamura S, Takamura T, Matsuzawa-Nagata N, et al. Palmitate induces insulin resistance in H4IIEC3 hepatocytes through reactive oxygen species produced by mitochondria. J Biol Chem 2009;284:14809–14818
4. Lionetti L, Mollica MP, Donizzetti I, et al. High-lard and high-fish-oil diets differ in their effects on function and dynamic behaviour of rat hepatic mitochondria. PLoS One 2014;9:e92753
5. Cavaliere G, Trinchese G, Bergamo P, et al. Polyunsaturated fatty acids attenuate diet induced obesity and insulin resistance, modulating mitochondrial respiratory uncoupling in rat skeletal muscle. PLoS One 2016;11:e0149033
6. Nedergaard J, Ricquier D, Kozak LP. Uncoupling proteins: current status and therapeutic prospects. EMBO Rep 2005;6:917–921
7. Tseng YH, Cypess AM, Kahn CR. Cellular bioenergetics as a target for obesity therapy. Nat Rev Drug Discov 2010;9:465–482
8. Diano S, Horvath TL. Mitochondrial uncoupling protein 2 (UCP2) in glucose and lipid metabolism. Trends Mol Med 2012;18:52–58
9. Li B, Nolte LA, Ju JS, et al. Skeletal muscle respiratory uncoupling prevents diet-induced obesity and insulin resistance in mice. Nat Med 2000;6:1115–1120
10. Haroon S, Vermulst M. Linking mitochondrial dynamics to mitochondrial protein quality control. Curr Opin Genet Dev 2016;38:68–74
11. Patel PK, Shirihai O, Huang KC. Optimal dynamics for quality control in spatially distributed mitochondrial networks. PLoS Comput Biol 2013;9:e1003108
12. Area-Gomez E, Del Carmen Lara Castillo M, Tambini MD, et al. Upregulated function of mitochondria-associated ER membranes in Alzheimer disease. EMBO J 2012;31:4106–4123
13. Schneeberger M, Dietrich MO, Sebastián D, et al. Mitofusin 2 in POMC neurons connects ER stress with leptin resistance and energy imbalance. Cell 2013;155:172–187
14. Zorzano A, Hernández-Alvarez MI, Sebastián D, Muñoz JP. Mitofusin 2 as a driver that controls energy metabolism and insulin signaling. Antioxid Redox Signal 2015;22:1020–1031
15. Detmer SA, Chan DC. Functions and dysfunctions of mitochondrial dynamics. Nat Rev Mol Cell Biol 2007;8:870–879
16. Liesa M, Palacín M, Zorzano A. Mitochondrial dynamics in mammalian health and disease. Physiol Rev 2009;89:799–845
17. Karlsson FH, Tremaroli V, Nookaew I, et al. Gut metagenome in European women with normal, impaired and diabetic glucose control. Nature 2013;498: 99–103
18. Turnbaugh PJ, Ley RE, Mahowald MA, Magrini V, Mardis ER, Gordon JI. An obesity-associated gut microbiome with increased capacity for energy harvest. Nature 2006;444:1027–1031
19. Neyrinck AM, Delzenne NM. Potential interest of gut microbial changes induced by non-digestible carbohydrates of wheat in the management of obesity and related disorders. Curr Opin Clin Nutr Metab Care 2010;13:722–728
20. Gao Z, Yin J, Zhang J, et al. Butyrate improves insulin sensitivity and increases energy expenditure in mice. Diabetes 2009;58:1509–1517
21. Mattace Raso G, Simeoli R, Russo R, et al. Effects of sodium butyrate and its synthetic amide derivative on liver inflammation and glucose tolerance in an animal model of steatosis induced by high fat diet. PLoS One 2013;8: e68626
22. Brown AJ, Goldsworthy SM, Barnes AA, et al. The orphan G protein-coupled receptors GPR41 and GPR43 are activated by propionate and other short chain carboxylic acids. J Biol Chem 2003;278:11312–11319
23. Davie JR. Inhibition of histone deacetylase activity by butyrate. J Nutr 2003; 133(7 Suppl.):2485S–2493S
24. Berni Canani R, Di Costanzo M, Leone L. The epigenetic effects of butyrate: potential therapeutic implications for clinical practice. Clin Epigenetics 2012;4:4
25. Pirozzi C, Lama A, Simeoli R, et al. Hydroxytyrosol prevents metabolic impairment reducing hepatic inflammation and restoring duodenal integrity in a rat model of NAFLD. J Nutr Biochem 2016;30:108–115
26. Iossa S, Mollica MP, Lionetti L, Crescenzo R, Botta M, Liverini G. Skeletal muscle oxidative capacity in rats fed high-fat diet. Int J Obes Relat Metab Disord 2002;26:65–72
27. Mollica MP, Trinchese G, Cavaliere G, et al. c9,t11-Conjugated linoleic acid ameliorates steatosis by modulating mitochondrial uncoupling and Nrf2 pathway. J Lipid Res 2014;55:837–849
28. Alexson SE, Nedergaard J. A novel type of short- and medium-chain acyl-CoA hydrolases in brown adipose tissue mitochondria. J Biol Chem 1988;263: 13564–13571
29. Hausladen A, Fridovich I. Measuring nitric oxide and superoxide: rate constants for aconitase reactivity. Methods Enzymol 1996;269:37–41
30. Flohé L, Otting F. Superoxide dismutase assays. Methods Enzymol 1984; 105:93–104
31. Barja G. Mitochondrial free radical production and aging in mammals and birds. Ann N Y Acad Sci 1998;854:224–238
32. Srere PA. Controls of citrate synthase activity. Life Sci 1974;15:1695–1710
33. Bergamo P, Maurano F, Rossi M. Phase 2 enzyme induction by conjugated linoleic acid improves lupus-associated oxidative stress. Free Radic Biol Med 2007;43:71–79
34. Levine RL, Garland D, Oliver CN, et al. Determination of carbonyl content in oxidatively modified proteins. Methods Enzymol 1990;186:464–478
35. Benson AM, Hunkeler MJ, Talalay P. Increase of NAD(P)H:quinone reductase by dietary antioxidants: possible role in protection against carcinogenesis and toxicity. Proc Natl Acad Sci U S A 1980;77:5216–5220

36. Habig WH, Jakoby WB. Assays for differentiation of glutathione S-transferases. Methods Enzymol 1981;77:398–405
37. Trinchese G, Cavaliere G, Canani RB, et al. Human, donkey and cow milk differently affects energy efficiency and inflammatory state by modulating mitochondrial function and gut microbiota. J Nutr Biochem 2015;26:1136–1146
38. Lama A, Pirozzi C, Mollica MP, et al. Polyphenol-rich virgin olive oil reduces insulin resistance and liver inflammation and improves mitochondrial dysfunction in high-fat diet fed rats. Mol Nutr Food Res 2016
39. Weibel ER, Kistler GS, Scherle WF. Practical stereological methods for morphometric cytology. J Cell Biol 1966;30:23–38
40. Altunkaynak BZ, Unal D, Altunkaynak ME, et al. Effects of diabetes and ovariectomy on rat hippocampus (a biochemical and stereological study). Gynecol Endocrinol 2012;28:228–233
41. Wan X, Xu C, Lin Y, et al. Uric acid regulates hepatic steatosis and insulin resistance through the NLRP3 inflammasome-dependent mechanism. J Hepatol 2016;64:925–932
42. Yamauchi T, Kamon J, Minokoshi Y, et al. Adiponectin stimulates glucose utilization and fatty-acid oxidation by activating AMP-activated protein kinase. Nat Med 2002;8:1288–1295
43. Minokoshi Y, Kim YB, Peroni OD, et al. Leptin stimulates fatty-acid oxidation by activating AMP-activated protein kinase. Nature 2002;415:339–343
44. Long YC, Zierath JR. AMP-activated protein kinase signaling in metabolic regulation. J Clin Invest 2006;116:1776–1783
45. Simeoli R, Mattace Raso G, Pirozzi C, et al. An orally administered butyrate-releasing derivative reduces neutrophil recruitment and inflammation in dextran sulphate sodium-induced murine colitis. Br J Pharmacol 2016
46. Meli R, Mattace Raso G, Calignano A. Role of innate immune response in non-alcoholic fatty liver disease: metabolic complications and therapeutic tools. Front Immunol 2014;5:177
47. Szendroedi J, Phielix E, Roden M. The role of mitochondria in insulin resistance and type 2 diabetes mellitus. Nat Rev Endocrinol 2011;8:92–103
48. Skulachev VP. Fatty acid circuit as a physiological mechanism of uncoupling of oxidative phosphorylation. FEBS Lett 1991;294:158–162
49. Korshunov SS, Skulachev VP, Starkov AA. High protonic potential actuates a mechanism of production of reactive oxygen species in mitochondria. FEBS Lett 1997;416:15–18
50. Osburn WO, Kensler TW. Nrf2 signaling: an adaptive response pathway for protection against environmental toxic insults. Mutat Res 2008;659:31–39
51. Schrepfer E, Scorrano L. Mitofusins, from mitochondria to metabolism. Mol Cell 2016;61:683–694
52. Bach D, Pich S, Soriano FX, et al. Mitofusin-2 determines mitochondrial network architecture and mitochondrial metabolism. A novel regulatory mechanism altered in obesity. J Biol Chem 2003;278:17190–17197
53. Kulkarni SS, Joffraud M, Boutant M, et al. Mfn1 deficiency in the liver protects against diet-induced insulin resistance and enhances the hypoglycemic effect of metformin. Diabetes 2016;65:3552–3560